Submission to the 29th International Symposium on Combustion,
Sapporo, Japan, July 2002

Prediction of Nitrogen Oxide Formation in Ammonia-Doped Turbulent Syngas Jet Flames

Torleif Weydahl,
Thermal Energy Department,
Sintef Energy Research, Trondheim, Norway

Ivar S. Ertesvåg, Inge R. Gran, Bjørn F. Magnussen
Department of Applied Mechanics, Thermodynamics, and Fluid Dynamics
Norwegian University of Science and Technology

and
Pia Kilpinen
Process Chemistry Group, Åbo Akademi, Åbo, Finland.

Author for correspondence:
Ivar S. Ertesvåg
Department of Applied Mechanics, Thermodynamics, and Fluid Dynamics
Norwegian University of Science and Technology
N-7491 Trondheim, Norway
fax: +47 73 59 35 80, phone: +47 73 59 38 39
e-mail: ivar.s.ertesvag@mtf.ntnu.no

Symposium Colloquium: 2. Pollutant Formation and Control
Symposium keywords: NOx, POLLUTANT KINETICS

Word count:

Total word count (max: 5500):	≈ 5300
Words in text:	≈ 2700
Figures (12×200):	2400
Equations with one line (2×21):	42
Lines in list of reference (22×7):	154

(Not included: Abstract and figure captions)

Abstract

Nitrogen-oxide formation from fuel-bound nitrogen in turbulent non-premixed flames was investigated. Calculations were performed using the k-ε model and a Reynolds-stress-equation model for turbulence and the Eddy Dissipation Concept for turbulent combustion (EDC) by Magnussen in conjunction with detailed chemistry of the chemical reaction mechanisms GRI Mech 3.0, GRI Mech 2.11, and Kilpinen97. The calculated case was a turbulent non-premixed syngas jet flame with ammonia added to the fuel, which was compared to experimental results reported in the literature. The results obtained for mean velocity, temperature, and mixture fraction agreed with the experimental data. Integrated values for NO formed from fuel-bound nitrogen were generally in good agreement with experimental data. This holds for all the three reaction mechanisms used. The GRI Mech 3.0 gave the highest, and the Kilpinen mechanism the lowest levels of nitrogen oxides. Furthermore, details of the chemistry of the turbulent flame were studied, and the most important elementary reactions for this case were identified when using the Kilpinen mechanism. The main path for NO formation was degradation of ammonia through NH. This conversion took place in the main part of the flame, to approximately 30 jet-nozzle diameters downstream. Throughout a longer zone, the jet flow down to approximately 100 diameters downstream, some of the NO reacted to HONO and further to NO_2 and both these species were emitted from the flame.

Introduction

The motivation for this work is the increasing concern related to emission of nitrogen oxides from fuels containing nitrogen, such as biomass and coal. Emission of nitrogen oxides (NO_x) is a serious threat to our environment: NO_x is the main source of acid rain, ground-level ozone, and contributes to photochemical smog. NO_x can be formed at a high temperature by fixation of N_2 in the combustion air. This is usually the main source of NO_x when oil or natural gas is burned, as these fuels often burn at very high peak temperatures. In biomass and coal combustion, fuel-bound nitrogen is the main source for NO_x emission. During gasification, fuel-bound nitrogen is mainly released in the form of hydrogen cyanide (HCN) and ammonia (NH_3) dependent on the gasifier type and process conditions. When these components take part in combustion with excess air, a considerable fraction is transformed to nitrogen oxides.

This work deals with comprehensive combustion modeling which has proven to be a useful tool for development of more efficient low-NO_x techniques. The specific aim of this study was to assess the ability of the Eddy Dissipation Concept (EDC) [1–5] for turbulent combustion with detailed chemistry to predict the conversion of ammonia to nitrogen oxides. For accurate NO_x predictions both the mixing model and the chemistry, and their coupling, need to be reasonable.

Experimental Data

The present simulations were compared with measurements performed by Lapp et al. [6] and later reported by Drake *et al.* [7]. The horizontal fuel jet, which emerged from a 3.2 mm diameter nozzle with an average flow of 54.6 m/s, was centered in a 0.15 m wide square channel with an air flow of 2.4 m/s. The composition of the fuel (on mole basis) was 39.7% CO, 29.9% H_2, 29.7% N_2, and 0.7% CH_4. Ammonia was added in amounts varying from 0.0% to 1.64%. Methane was not included in the gas mixture when ammonia added was zero. Laser velocimetry and pulsed Raman scattering provided data for mean and rms of velocity, temperature, and major species concentrations. The formation of nitric oxide (NO) was experimentally analyzed by probe sampling 100 diameters downstream of the nozzle outlet.

Modeling

The turbulent reacting flow was modeled by the mass-weighted Reynolds-averaged (Favre-averaged) conservation equations for momentum components, energy, and mass of all individual species. Both the standard k-ε model and a Reynolds-stress-equation model were used as turbulent closure. The models were employed with an adjusted constant in the ε equation ($C_{\varepsilon 2}$=1.83) to fit the velocity field for the round jet. For turbulent transport of energy and species mass, the general gradient model was used. The turbulence Prandtl and Schmidt numbers were set to 0.5, which in this case gave the best fit to the radial mixture-fraction profiles.

The Eddy Dissipation Concept for turbulent combustion (EDC) [1–5] by Magnussen was used to model the interaction between turbulence and combustion. The chemical reactions are assumed to occur in the fine structures, *i.e.* the small turbulence scales. The mass exchange is the reciprocal of the fine-structure residence time, $\tau^* = 1/\dot{m}^*$, which is proportional to the Kolmogorov time scale. The implementation of chemical kinetics is described in Ref. [3]. Then, the mean reaction rate for a chemical species is expressed as

$$\overline{R}_k = \bar{\rho}\widetilde{\omega}_k = -\bar{\rho}(\gamma^*)^{2/3}\dot{m}^*(Y_k^\circ - Y_k^*). \tag{1}$$

Here, Y_k° and Y_k^* are the mass fraction of species k entering into and leaving the fine-structure reactor, respectively. The quantities $\gamma^* = 9.8(\nu\varepsilon/k^2)^{3/4}$ and $\dot{m}^* = 2.5(\varepsilon/\nu)^{1/2}$ are the mass fraction of turbulence fine structures and its mass exchange with the surrounding fluid, respectively. These are related to the turbulence-cascade model of the EDC [4,5]. The reacting turbulence fine structure is regarded as a perfectly stirred reactor, and the mass balance in the reactor is expressed as

$$dY_k/dt = \omega_k^* + \nu_r(Y_k^\circ - Y_k^*) \tag{2}$$

for each species k. Here, the reactor mixing rate is $\nu_r = 1/\tau^*$, and $\omega_k^* = R_k^*/\rho^*$ is the chemical reaction rate term. These species mass balances, together with balances for energy and momentum, are solved for the reactor by integrating to steady state. The contribution to the reaction rate from each elementary reaction can be identified.

The reaction rate ω_k^* was calculated with detailed-chemistry data obtained from three different reaction mechanisms: GRI-Mech 2.11 [8], GRI-Mech 3.0 [9], and the mechanism by Kilpinen [10]. These mechanisms involve 277, 325, and 353 elementary reactions between 49, 53, and 57 chemical species, respectively.

The reactions included are the oxidation of simple hydrocarbons (C_1 – C_3), HCN, and NH_3 as well as interactions between hydrocarbon radicals and nitrogen species (NO, NH_x, N_2). The GRI mechanisms have been especially developed for prediction of natural-gas flame propagation and ignition. For the Kilpinen mechanism, the main focus has been on nitrogen chemistry at fluidized-bed combustion and diesel-engine conditions.

The predictions were made using the general-purpose CFD code Spider, which is based on finite volumes and a non-orthogonal curvilinear computational grid [11, 12]. In this case, a two-dimensional rectangular mesh with axial symmetry was used. Hence, the effect of buoyancy on the horizontal flame was not accounted for.

A simple radiation model [13] was applied for the major species. This model assumes an optically thin flame, and mean values of temperature and species concentration were used.

Results for the flow and concentration field

Predicted results for axial velocity were generally in satisfactory agreement with measurements. It is known that the standard k-ε turbulence model over-predicts the spreading of a round jet. The modification mentioned above resulted in improved predictions, which more closely matched the dataset. Nevertheless, the mixture-fraction profiles through the flame were in varying agreement. Figure 1 presents a comparison of measurements [7] and predictions of mixture fraction at two distances from the nozzle outlet. Here, the mixture fraction was determined on the basis of hydrogen elemental mass. The profile at $x/d = 50$ shows only minor deviations from the experiments, whereas calculated values at $x/d = 10$ were more spread than in the experiments. Here, d is the internal diameter of the nozzle, x is the axial distance from the nozzle outlet, and y (in the figures) is the radial distance from the axis of symmetry.

Velocity profiles from computations and experiments are shown in Fig. 2 for $x/d = 25$ and $x/d = 100$, and the centerline development is shown in Fig. 3. Figure 4 shows measurements and predictions of temperature at $x/d = 100$. The calculated profile is less spread than the experimental profile. The velocity, temperature and mixture-fraction results did not differ significantly between the three chemical mechanisms used in this study. Furthermore, they were not affected by the small amounts of ammonia or methane added. The mean flow and scalar fields obtained with the Reynolds-stress-equation model did not differ considerably from those of the k-ε model and are therefore not presented here.

The upstream boundary coincides with the nozzle outlet and the jet-nozzle inlet profiles were taken from a separate computation a fully developed pipe-flow. However, this case has been compared to simulations where the fuel-jet tube, the fuel flow inside it, and the air flow outside it were included in an extended calculation domain. The results from these two approaches were very close to each other. The air-coflow channel wall was approximated as a cylindrical wall. It was found that the position of this wall did not affect the combusting-flow results.

Figure 5 shows the comparison of measurements and predictions of NO at $x/d = 100$ for 0.8% ammonia addition. Results from the three chemical mechanisms are shown. The calculated profiles are less spread than the experimental profile, corresponding with the temperature profile in Fig. 4. However, the differences between the mechanisms are greater than their deviations from experimental data. Nevertheless, the level of NO is close to that of the experiments.

Figure 6 shows the peak values, *i.e.* the jet-centerline values, of the NO concentration at $x/d = 100$ for five different amounts of ammonia added to the fuel. Results are shown for the three chemical mechanisms together with experimental data [7]. Also curve fits through the results are included for each mechanism.

The corresponding total amount of NO is shown in Fig. 7 as a fraction of the amount of ammonia added to the fuel. Here, the NO flux at $x/d = 100$ was integrated over a cross section and divided by the amount of inflow NH_3.

Both these two figures and Fig. 5 show that the GRI Mech 3.0 gave the highest, and the Kilpinen mechanism the lowest levels of NO. When NO_2 was included, the picture observed was very much the same (not shown in the figures). At $x/d = 100$, the NO_2 flux was approximately 15 % of the NO flux. In addition, the Kilpinen mechanism predicted a small amount of HONO (approx. 6% of the NO flux). This species is not included in GRI Mech 2.11 and 3.0.

The differences seen between the three mechanisms are also demonstrated in Fig. 8, which shows the downstream development of the molar flow of NO_x integrated over a cross section. Here, and in the following, NO_x includes NO, NO_2, and N_2O. However, the amount of N_2O was negligible. Results for the three chemical mechanisms are shown for 0.8% added ammonia (upper curve set), and with no added ammonia or methane, *i.e.* thermal NO_x only (lower curve set). This figure shows that the addition of ammonia, *i.e.* fuel nitrogen, caused the major contribution to NO_x formation. This is consistent with the experimental data shown in Fig. 6. In the first 30 diameters downstream, the net production of NO_x was mainly NO. At this distance, the maximum level was reached. From this point, some of the NO was converted to NO_2 and, with the Kilpinen mechanism, also to HONO.

As seen in Fig. 8, a substantial part of the NO_x was produced in the first part of the jet, that is, less than 3 nozzle diameters downstream from the nozzle. This holds for all three mechanisms. However, it is also seen that the major differences between the three mechanisms were developed in the range from approximately 3 to 30 diameters downstream. In the figure, this can be seen by the different slopes of the three upper curves in the interval of x/d from 3 to 30.

The results of the NO_x formation and reduction are promising, and the agreement between computations and experiments is satisfactory. A further step in the study was to investigate the detailed effects of the chemical mechanisms. This detailed knowledge will be useful in developing improved combustion devices, such as low-NO_x wood stoves and waste incinerators.

Details of the reaction-rate fields

Controlling the NO_x formation in combustion devices requires detailed knowledge of the reaction paths and of the properties affecting these in the turbulent reacting flow.

The results shown in Figs. 9 *et seq.* point towards a possible approach in studying the details of the conversion of ammonia and other species in turbulent combustion. Here, results of the Kilpinen mechanism will be shown. The presented results were obtained for 0.8% ammonia added to the fuel. The graphs represent the radially integrated generation rate of NO_x for specific reversible elementary reactions as well as the net contribution from a set of such reactions. The directions of the one-way arrows in the figures correspond to positive production rates in the graphs. The individual contributions of all elementary reactions involving NO_x were compared.

Figure 9 shows the development of the total production rate of NO_x (*i.e.* NO, NO_2, and N_2O) from $x/d = 3$. The net contribution from the nine most important elementary reactions is also shown. These reactions will be discussed subsequently. The difference between the two curves here shows the contribution from the remaining elementary reactions involving NO_x.

The downstream development of NO production by two important reactions is shown in Fig. 10. These are two of the Zeldovich reactions usually responsible for thermal NO formation. However, in this case, these reactions can also be related to the breakdown of NH_3 in the flame. The third Zeldovich reaction, formation of NO from N and O_2, did not

contribute significantly in this instance.

Three reactions involving NH are shown in Fig. 11. These reactions were important in the breakdown of NH_3, and involved also an exchange between NO and NO_2. Two of these reactions nearly counterweight each other in the NO_x balance, and the net contribution is close to, but not equal to the reaction of NH with O. The net contribution to NO_x was always positive and was the most important contribution from 7 to 15 diameters downstream. The Zeldovich reactions described above had a negative contribution up to 10 diameters, and was the most important positive contribution from 15 to 30 diameters downstream from the nozzle.

Figure 12 shows the contribution from four reactions involving HONO. These reactions had a significant contribution, consuming NO all the way down to 110 diameters downstream. Thus, a small amount of HONO was released from the flame. As described above, the reactions in Figs. 10–12 are summarized and compared with the total production rate of NO_x in Fig. 9.

The main reaction path forming nitrogen oxides, throughout the three-dimensional turbulent flame, appeared to be a breakdown of NH_3 to NH, which formed NO as shown in Fig. 11. Some of the NO was converted through HONO to NO_2. For an interval a few diameters from the nozzle, N_2 formation from NO was important, and thus reducing the NO level. N_2 was also formed from N_2O through NH and NO.

Discussion

The turbulence models available are well known to overpredict the spreading rate of jet flames, leading to too low maximum values. This is to some extent remedied by simple modifications of the model constants. Actually, the standard version of the k-ε model turbulence model predicts a lower peak temperature, and therefore less thermal NO production. With that model version, however, the velocity field was not so well predicted. Since the round jet also presents a considerable challenge for newer, more complex turbulence models, the solution may be an *ad-hoc* jet-flame turbulence model designed specifically for combustion model development. When the purpose is to investigate details of the combustion field, it is adequate to do such modifications to the flow-field model. On this background, the results obtained for mean velocity, temperature, and species concentration can be regarded as satisfactory compared with experiments, and the deviations observed were as expected.

The peak mean temperatures were somewhat overpredicted, resulting in too high thermal NO formation. However, when fuel nitrogen is present, it is the major source of nitrogen oxides, and this formation mechanism is less sensitive to the temperature than the thermal NO formation. The temperature is affected by thermal radiation, and some of the temperature overprediction can be related to possible deficiencies in the radiation modeling. Furthermore, overprediciton of temperature also indicates that the reactions were predicted to occur too close to the nozzle. This in turn may be attributed to the higher temperature, thus making this a self-enhancing process. Some of the discrepancy, in particular far downstream, can be explained by the deviation from axisymmetry of the horizontal experimental flame due to buoyancy.

Concluding Remarks

A turbulent non-premixed jet flame with ammonia added to the fuel has been computed using the Magnussen's Eddy Dissipation Concept for Turbulent combustion. Detailed chemistry was modeled with data from three different chemical mechanisms, that is the GRI Mech 3.0, the GRI Mech 2.11, and the Kilpinen97 mechanism.

The results obtained for mean velocity, temperature, and mixture fraction agreed with the experimental data. Integrated values for NO formed from fuel-bound nitrogen were generally in good agreement with experimental data. This holds for all the three reaction mechanisms used. The GRI Mech 3.0 gave the highest, and the Kilpinen mechanism the lowest levels of NO and NO_x.

It was demonstrated how the computational model allows detailed investigation of the chemistry of the turbulent flame. The most important elementary reactions for this case was identified. Such knowledge is of great importance in the design of new, low-NOx combustion equipment. In the computations with the Kilpinen mechanism, the main path for NO formation was degradation of ammonia through NH. Some of the NO reacted to HONO and further to NO_2.

Acknowledgments: We are grateful to our colleague Andrea Gruber, Sintef Energy Research, for performing some of the computations of this study.

References

[1] Magnussen, B.F. "Modeling of NO_x and soot formation by the Eddy Dissipation Concept." Int. Flame Research Foundation, 1st Topic Oriented Technical Meeting, 17-19 Oct. 1989, Amsterdam, Holland.

[2] Gran, I.R., Magnussen, B.F., Comb. Sci. Technol. 119: 171 (1996).

[3] Gran, I.R., Magnussen, B.F., Comb. Sci. Technol. 119: 191 (1996).

[4] Ertesvåg, I.S., Magnussen, B.F., Comb. Sci. Technol. 159: 213 (2000).

[5] Ertesvåg, I.S., "Turbulent flow and combustion" (In Norwegian), Tapir Academic Publisher, Trondheim (2000).

[6] Lapp, M., Drake, M.C., Penney, C.M., Pitz, R.W., Correa, S., "Turbulent Combustion Experiments and Modeling." Final Report prepared for Power Systems Division, U.S. Dept. Energy, Washington D.C. (1983).

[7] Drake, M.C., Pitz, R.W., Correa, S.M., Lapp, M,. Proc. Comb. Inst. 28:1983 (1984).

[8] Bowman, C.T, Hanson, R.K., Davidson, D.F., Gardiner Jr., W.C., Lissianski, V., Smith, G.P., Golden, D.M., Frenklach, M., Goldenberg, M., "Gri-Mech 2.11" `http://www.me.berkeley.edu/gri_mech/` (1999).

[9] Smith, G.P., Golden, D.M., Frenklach, M., Moriarty, N.W., Eiteneer, B., Goldenberg, M., Bowman, C.T., Hanson, R.K.,Song, S., Gardiner Jr., W.C., Lissianski, V.V., and Qin, Z., "Gri-Mech 3.0" `http://www.me.berkeley.edu/gri_mech/` (2000).

[10] Kilpinen, P., "KILPINEN97", `http://www.abo.fi/fak/ktf/cmc/research` (1997).

[11] Melaaen, M.C., Num. Heat Transf. B 21: 1 (1992).

[12] Melaaen, M.C., Num. Heat Transf. B 21: 21 (1992).

[13] "Computational Submodels (Updated 7-JUN-2000)" Int. Workshop on Meas. and Comput. of Turbulent Nonpremixed Flames, `http://www.ca.sandia.gov/tdf/Workshop/Submodels.html`

List of Figures

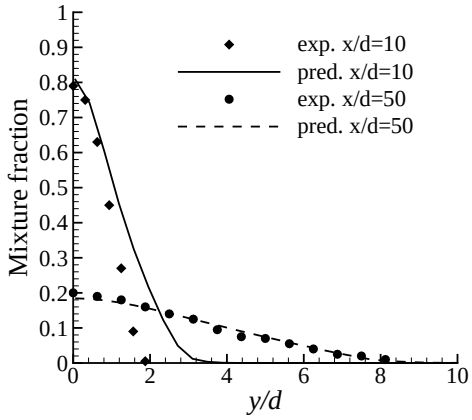

Figure 1: Comparison of measurements [7] and predictions of mean mixture fraction at x/d=10 and x/d=50. These and the following mean velocity and temperature results were virtually equal for all three chemical mechanisms investigated.

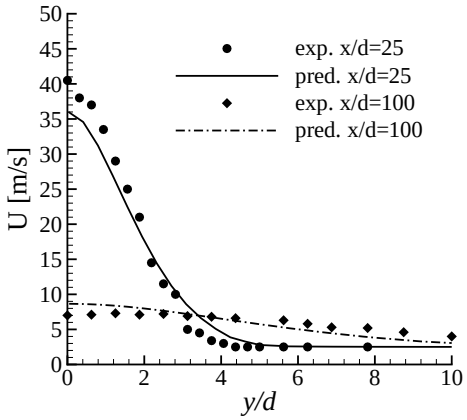

Figure 2: Mean velocity profiles, cf. Fig. 1.

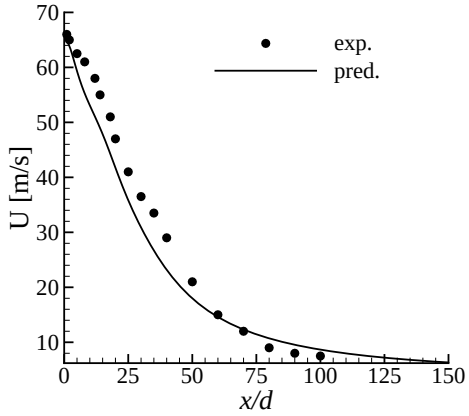

Figure 3: Centerline mean velocity, cf. Fig. 1.

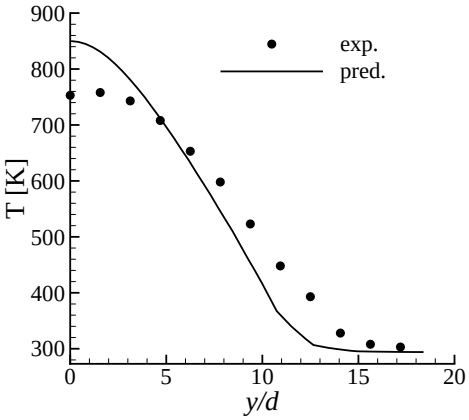

Figure 4: Mean temperature at $x/d = 100$, cf. Fig. 1.

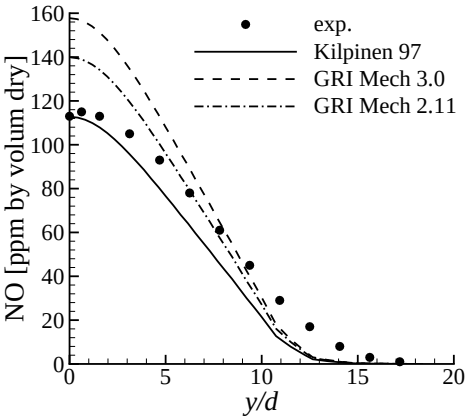

Figure 5: Comparison of measurements [7] and predictions of NO at $x/d = 100$ with 0.8% NH_3 added to the fuel. Results from three chemical mechanisms.

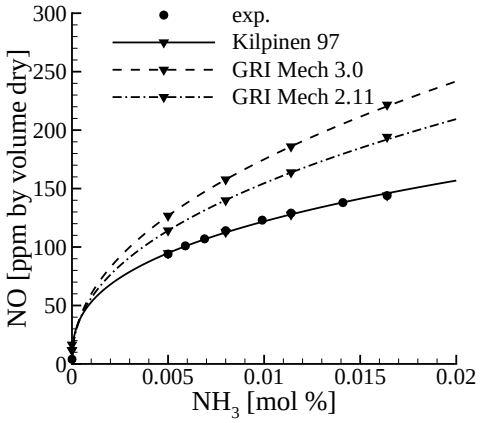

Figure 6: Comparison of measurements [7] and predictions for the molar yield of NO from NH_3. Peak values of NO at $x/d = 100$ for various amounts of added NH_3 and curve fits between the specific amounts for each of the three mechanisms.

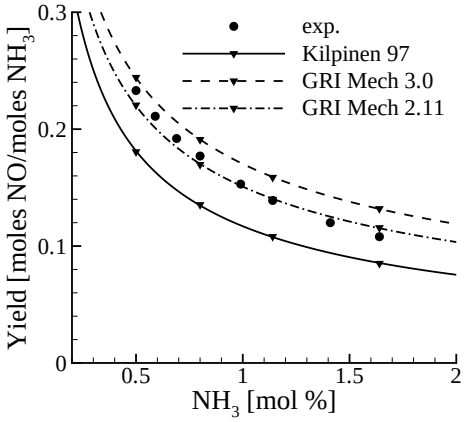

Figure 7: Radially integrated values of NO at $x/d = 100$, cf. Fig. 6.

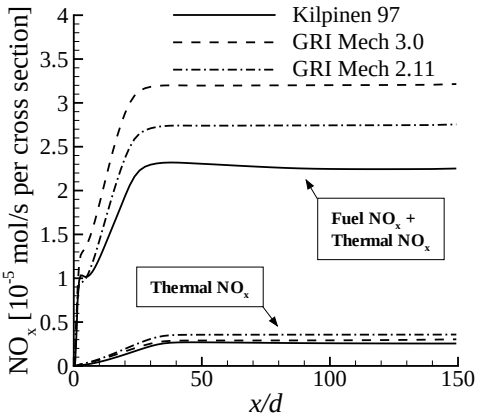

Figure 8: Downstream development of NO_x (NO, NO_2, and N_2O) molar flow. Radially integrated molar flows of NO_x for 0.8% ammonia added to the fuel (upper curve set), and with no ammonia or methane added (thermal NO_x, only) (lower curve set). Comparison of the three chemical mechanisms.

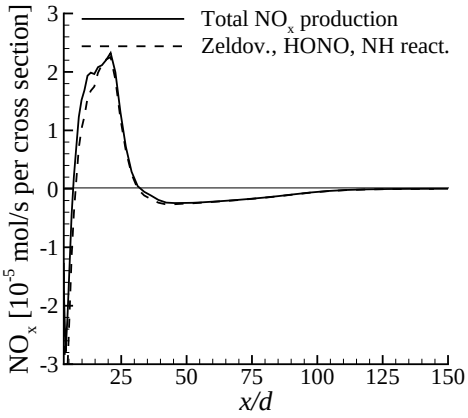

Figure 9: Radially integrated total production rate of NO_x, compared to the net contribution from the nine most important elementary reactions, cf. Figs. 10–12. Results from the Kilpinen mechanism.

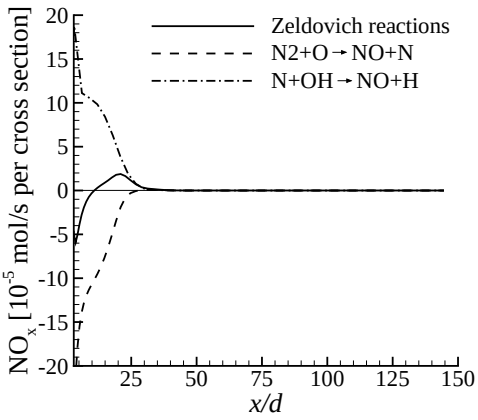

Figure 10: Contribution to the production rate of NO_x from two important elementary reaction, and the sum of these two reactions. Radially integrated production rates with the Kilpinen mechanism.

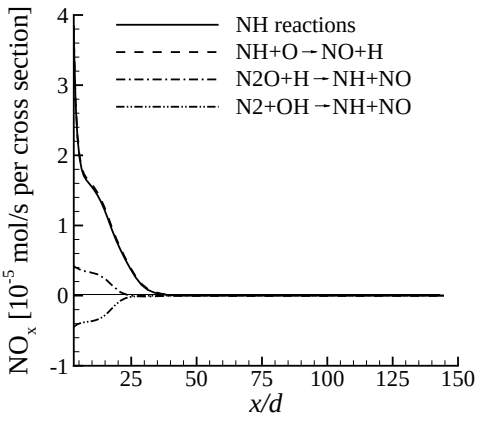

Figure 11: Contribution from three reactions involving NH, cf. Fig. 10.

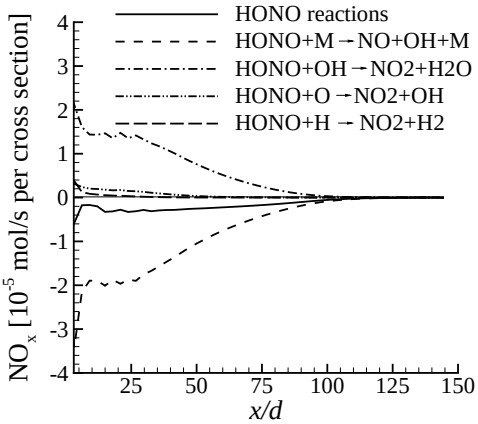

Figure 12: Contribution from four reactions involving HONO, cf. Fig. 10.